SOFT ROBOTICS
Volume 0, Number 0, 2021

DOI: 10.1089/soro.2021.0080

SoRo
Soft Robotics

Fast Thermal Actuators for Soft Robotics

Shuang Wu,[1] Gregory Langston Baker,[1] Jie Yin,[1] and Yong Zhu[1–3,i]

Abstract

Thermal actuation is a common actuation method for soft robots. However, a major limitation is the relatively slow actuation speed. Here we report significant increase in the actuation speed of a bimorph thermal actuator by harnessing the snap-through instability. The actuator is made of silver nanowire/polydimethylsiloxane composite. The snap-through instability is enabled by simply applying an offset displacement to part of the actuator structure. The effects of thermal conductivity of the composite, offset displacement, and actuation frequency on the actuator speed are investigated using both experiments and finite element analysis. The actuator yields a bending speed as high as 28.7 cm^{-1}/s, 10 times that without the snap-through instability. A fast crawling robot with locomotion speed of 1.04 body length per second and a biomimetic Venus flytrap were demonstrated to illustrate the promising potential of the fast bimorph thermal actuators for soft robotic applications.

Keywords: silver nanowires, soft robot, soft actuator, snap-through instability, electrothermal actuation

Introduction

Soft robots are constructed from highly compliant materials. In contrast to their rigid counterparts, they allow adaptability to changing environments and dynamic task settings, as well as improved safety when working around humans.[1,2] Soft robots have found wide applications in biomedical engineering, surgical assistance, active prosthetics, camouflage, and perception technologies.[3–7] Researchers have been exploring different actuation methods for soft robots using a variety of stimuli, including pressure,[8,9] heat,[10,11] electrical field,[12–14] magnetic field,[15–17] and chemical potential.[18,19]

No actuation method has yet emerged as the dominant method. Trade-offs exist in force, speed, displacement, and requirement for auxiliary equipment. Research in the field has so far focused on improving the performances of these actuation methods.[2] Among the various types of stimuli, electric stimulus is one of the simplest and most convenient, where electroactive polymers, either ionic or field activated, are widely used. For electrically stimulated actuators, the ionic activation typically operates in an electrolyte environment while the field activation requires high voltage (>1 kV).[20]

Another type of electrically stimulated actuator, bimorph thermal actuator,[10,21,22] based on mismatch in coefficient of thermal expansion (CTE) of two materials, has drawn much attention due to programmable operation,[23] lightweight, low actuation voltage, being electrolyte free, and potential for untethered operation (e.g., using wireless charging).[24,25] However, owing to the intrinsic thermal properties of soft materials, a major limitation of such thermally triggered soft robots is the relatively low speed. Indeed, improving the speed of soft robots has been a general challenge in the field,

Departments of [1]Mechanical and Aerospace Engineering and [2]Materials Science and Engineering, North Carolina State University, Raleigh, North Carolina, USA.
[3]Joint Department of Biomedical Engineering, University of North Carolina-Chapel Hill and NC State University, Chapel Hill, North Carolina, USA.
[i]ORCID ID (https://orcid.org/0000-0002-3862-5757).

especially for entirely soft robots (without assistance of rigid skeletons, frames, etc.).[13,26,27]

An intuitive way to enhance the speed of an electrothermal actuator is to increase the thermal conductivity (TC) of the stimuli-responsive materials. However, the enhancement of TC of soft materials is generally limited within a factor of 2.[28] In addition to the material-based strategy, instability-based shape morphing has attracted much attention.[29] Snap-through instability has been adopted in the field of soft actuators and soft robots,[30–34] due to its ability to trigger sudden and large deformations.[35]

A soft acrylic membrane being inflated near the onset of instability showed a increase of 1692% in area within 150 s (over 200 times faster than without instability).[34] A soft bistable valve was reported to switch between different states using pneumatic pressure triggered snap-through instability.[36] In another work, a soft actuator composed of interconnected fluidic segments harnessed snap-through instability to amplify the changes in internal pressure, extension, shape, and exerted force.[32] For locomotion robots, a spine assisted soft crawling robot leveraging the elastic instability was reported with high locomotion speed and large actuation force.[33] However, the combination of snap-through instability with soft electrothermal actuation has not been reported for designing high-performance, entirely soft robots.

In this study, we present a bimorph thermal actuator, based on a silver nanowire/polydimethylsiloxane (AgNW/PDMS) composite, with snap-through instability to achieve fast actuation.

The actuator, including two active and one passive ribbons, was fabricated using a simple and low-cost process (Fig. 1). The snap-through instability was introduced by applying an offset displacement to the passive ribbon. Both experiments and finite element analysis (FEA) were conducted to investigate the effects of thermal conductivity of the AgNW/PDMS composite, offset displacement, and actuation frequency on the actuator performance. The snap-through instability significantly increased the actuation speed, up to 10 times that without the instability. A fast crawling robot with locomotion speed of 1.04 body length per second (BL/s) and a biomimetic Venus flytrap were demonstrated to illustrate the promising potential of the fast bimorph thermal actuators for soft robotic applications.

Materials and Methods

Fabrication of snap-through enabled AgNW actuator

First, 60 mL of a 0.147 M Polyvinylpyrrolidone (PVP) (MW ~40,000; Sigma-Aldrich) solution in ethylene glycol (EG) was added to a round-bottom flask to which a stir bar was added; the vial was then suspended in an oil bath (temperature 151.5°C) and heated for 1 h under magnetic stirring (150 rpm). Then at 1 h, 200 μL of a 24 M $CuCl_2$ ($CuCl_2 \cdot 2H_2O$, 99.999+%; Sigma-Aldrich) solution in EG was injected into the PVP solution. The solution was then injected 60 mL of a 0.094 M AgNO3 (99+%; Sigma-Aldrich) solution in EG.

The AgNW solution was drop-casted on plasma treated glass slide; at the same time, the solution was heated by a hot plate at 50°C to evaporate the solvent. Then liquid PDMS (SYLGARD 184; DOW, Inc.) with a weight ratio of 10:1 was mixed thoroughly with Barium Titanate (BT) powder (weight ratio 80%) before spin coating onto the AgNW film. The coated composite precursor was cured at 100°C for 1 h. The cured composite film was then laser cut into an M shaped pattern and removed from the glass slide. Then the AgNW/BT/PDMS composite film was attached to a fixed supporting surface with the middle ribbon slightly dislocated in the horizontal direction. Cu wires were attached to the two outer ends of the pattern by silver epoxy (MG Chemicals) for connection to the power source.

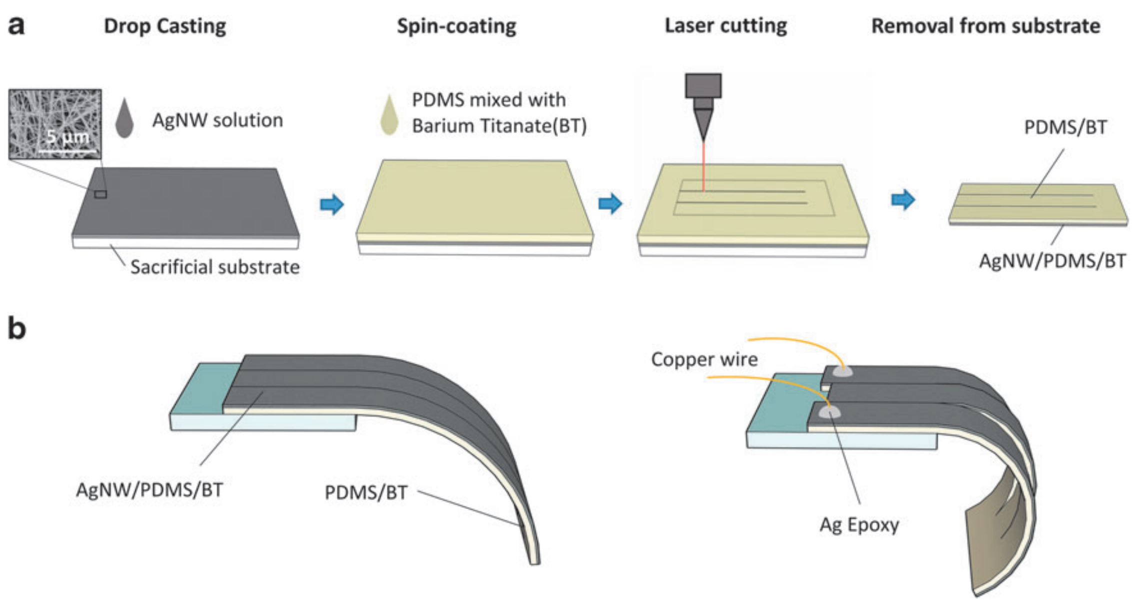

FIG. 1. Design of the bimorph thermal actuator. **(a)** Fabrication process of the bimorph thermal actuator. **(b)** Schematic view of the bimorph thermal actuators without (*left*) and with (*right*) offset displacement on the passive ribbon. AgNW, silver nanowire; PDMS, polydimethylsiloxane. Color images are available online.

Fabrication of snap-through enabled crawling robot

The AgNW/BT/PDMS composite film was prepared using the same materials and method described above. Then the composite film was laser cut into an M shaped pattern with four extended limbs at the four corners. The middle ribbon was slightly dislocated in the horizontal direction and then fixed together with the other two ribbons by a piece of adhesive tape. Cu wires were attached to the two outer ends of the pattern by silver epoxy (MG Chemicals) for connection to the power source (Agilent 6613C).

Fabrication of snap-through enabled Venus flytrap

The AgNW/BT/PDMS composite film was prepared using the same materials and method described above. Then the composite film was laser cut into a biomimetic Venus flytrap shaped leaf. The flytrap was finished by having two of the fabricated leaves facing each other and applying offset on the middle ribbon. Finally, Cu wires were attached to the two outer ends of the two leaves by silver epoxy (MG Chemicals) for connection to the power source (Agilent 6613C).

Measurements

Temperature change of the stretchable thermochromic heater was measured with an infrared camera (A655SC FLIR) with error of ±2°C or ±2% of reading.

Results and Discussion

Figure 1a shows the fabrication process of the snap-through enabled bimorph thermal actuator. AgNWs have been widely used as a heating material in soft devices due to their excellent electric conductivity and mechanical compliance.[10,37–41] In this work, we fabricated the soft actuator using the AgNWs in the form of a percolation network, as the heating element, embedded just below the surface of the polymer matrix (PDMS in this case).[42–44] The AgNW/PDMS layer (3 μm in thickness) and the pure PDMS layer (50 μm in thickness) form a thermal bimorph.

During the fabrication, BT powders (with average diameter of 6.08 μm) were doped into the precursor of PDMS to enhance the thermal conductivity (Supplementary Fig. S1). The weight ratio of BT and PDMS, 0.8, was used in this work. The TC of PDMS/BT increased from 0.15 W/mK (derived from the data sheet of SYLGARD 184; DOW, Inc.) to 0.23 W/mK. After curing in an oven, the composite film was laser cut into an M shaped pattern (16×6 mm) with three ribbons connected at one end but separated at the other (Fig. 1a). The two outward ribbons together with the connecting part of the M shaped pattern form the conducting path with uniform sheet resistance.

When applying a low voltage (on the order of a few volts) at the two ends of the ribbons, the conducting path of the composite film can quickly heat up (e.g., 120°C within 14 s at 2 V) (Supplementary Fig. S2a). From Supplementary Figure S2b, a decrease of time constant from 2.64 to 1.73 s can be seen when comparing the cases without and with doping of BT powders. To reach a certain temperature, the heating time can be reduced under a higher voltage (Supplementary Fig. S2a). Thus we chose 2 V in the rest of this work to illustrate the low-voltage actuation. Higher voltage may introduce local overheating due to possible nonuniformity in the AgNW network as a result of the drop-casting method used in this work. Printing can achieve more uniform AgNW network.[45,46]

To increase the actuation speed, we introduced a snap-through mechanism by applying an offset displacement at the free end of the middle ribbon, as shown schematically in Figure 1b. The offset ratio δ is defined as the ratio of the offset displacement of the middle ribbon to the length of the middle ribbon.

When peeled off from a sacrificial substrate, the composite film automatically curled (with the initial curvature of $-5.23\,\mathrm{cm}^{-1}$) due to the stress gradient in the PDMS introduced during the curing. The middle ribbon is curved, with a curvature, slightly different from the initial one, after introducing the offset displacement. Upon turning on the voltage, the outward ribbons heat up as a result of Joule heating and undergo a typical bimorph thermal actuation as a result of the CTE mismatch between the AgNW/PDMS and PDMS layers. In this study, the AgNW density was $0.5\,\mathrm{mg/cm}^{-2}$ (CTE of AgNW/PDMS composite $1.9 \times 10^{-4}\ \mathrm{K}^{-1}$, according to Supplementary Fig. S3); by contrast, CTE of PDMS is 3.1×10^{-4} K^{-1} (from Dow Product information sheet of SYLGARD 184).

The CTE of AgNW/PDMS composite as a function of the AgNW density is shown in Supplementary Figure S3. We define the two outward ribbons (thermally actuated) as the active ribbons while the middle ribbon as the passive ribbon.

During Stage I of the actuation (Fig. 2a①, ②), the passive ribbon gradually buckles up along with the active ribbons. Stage II (Fig. 2a②, ③) starts when the temperature on the active ribbons reaches the high transition temperature T_H. The stored strain energy triggers a sudden snap through (snap forward) on the passive ribbon. In this stage, the curvature of the passive ribbon snaps from negative (curve down) to positive (curve up) and as a result the entire composite film flips abruptly. Stage III (Fig. 2a③, ④) starts when the power is turned off. The temperature on the active ribbons gradually decreases, and the two active ribbons bend back toward the negative direction. The bending of the active ribbons again results in energy accumulation in the passive ribbon. Stage IV (Fig. 2a④–⑥) starts when the temperature on active ribbons drops to the low transition temperature T_L.

The second snap through (snap back) is triggered by the stored strain energy, which brings the whole structure eventually back to its initial state.

Figure 2b–d shows the temperature of the active ribbon and the curvature and bending speed of the passive ribbon (with 2% offset), respectively, under five steady-state cycles of power on and off (2 V). Temperature of the actuator was measured from the top AgNW/PDMS composite layer. And the curvature of the passive ribbon was measured using a camera with high frame rate (240 fps). Figure 2c shows that each cycle takes ~ 1 s for both forward and backward actuation. Of note is that the first cycle of heating up takes a bit longer time (~ 2 s) since the active ribbons have to heat up from room temperature (~ 23°C) to the first transition temperature (~ 100°C) (Supplementary Fig. S4). In the following cycles the time intervals are shortened by controlling the maximum and minimum temperatures in each cycle.

The two transition temperatures T_L (~ 76°C) and T_H (~ 88°C), as marked on Figure 2b, indicate the working temperature range for both the snap-forward and snap-back instabilities. In one actuation cycle, the two transition temperatures T_L and T_H must be reached, which is dictated by the

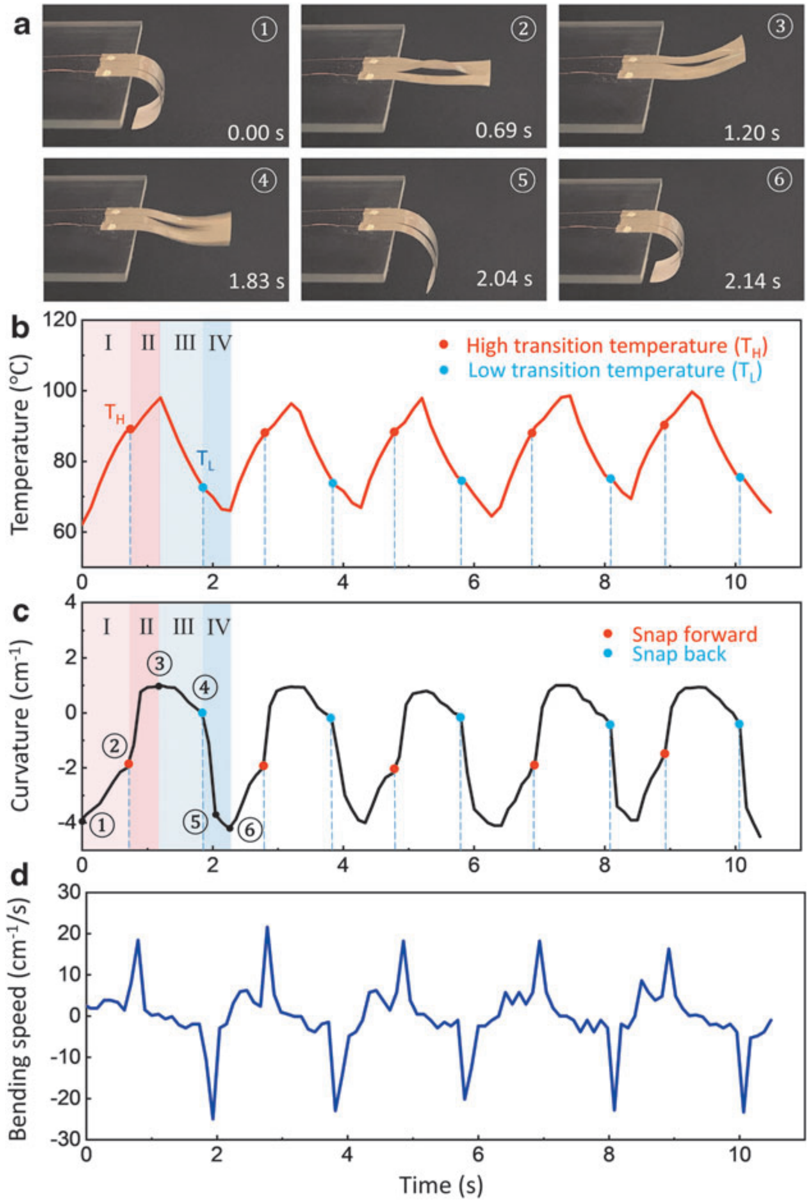

FIG. 2. Bending performance of the snap-through enabled bimorph thermal actuator. **(a)** Snapshots of the bimorph thermal actuator within one actuation cycle. **(b)** Temperature and **(c)** curvature of the snap-through enabled bimorph thermal actuator in five stable cycles. **(d)** Bending speed of the snap-through enabled bimorph thermal actuator. Color images are available online.

heat transfer characteristics of the bimorph structure. Within this constraint, we can control the actuation frequency and hence the actuation speed. In this work we chose 0.47 Hz square wave for the power supply. Figure 2d shows the bending speed of the actuator, which is calculated by taking the derivative of recorded curvature of the middle ribbon.

We first studied the effect of offset ratio δ. Figure 3a shows the curvatures of the actuators with different δ during one cycle of power on and off (square wave). The inset photographs compare the optimal case ($\delta = 2.75\%$) and the no-offset case ($\delta = 0\%$) side by side at three stages.

The curvature of 0% δ starts with a linear increase (at the speed of 4.1 cm^{-1}/s) until it reaches saturation, then decreases immediately (at the speed of 2.7 cm^{-1}/s) when the power is turned off. In this case, the bending performance is the same as a previously reported work using AgNW/PDMS heater for bimorph actuators[10] because the effect of the passive ribbon is negligible. The case of $\delta = 1\%$ shows a similar behavior. For the cases with $\delta = 2\%$, 2.5%, and 2.75%, the snap-forward and snap-back processes are clearly manifested. In the case of 2.75%, the initial bending speed is 4.6 cm^{-1}/s. Then the speed slows down to almost zero as the strain energy is being accumulated to overcome the negative curvature of the passive ribbon.

When the temperature rises to T_H, the snap-forward triggered bending speed increases to 17.3 cm^{-1}/s, which is 4.2 times that of the initial loading speed in the no-offset case. After turning off the power, the snap-back bending speed reaches 28.7 cm^{-1}/s, which is 10 times that of the unloading speed in the no-offset case. Such a significant improvement in actuation speed has not been reported for soft electrothermal actuators, to the best of our knowledge. It can be seen that with larger offset δ, the preparation time for snap through is longer and the peak loading and unloading speeds are larger. This is because of the larger δ, the larger the energy barrier to overcome, and the more energy that is released. However, when δ exceeds 3%, the energy barrier becomes insurmountable, and as a result, the actuator cannot go through the snap-through stage.

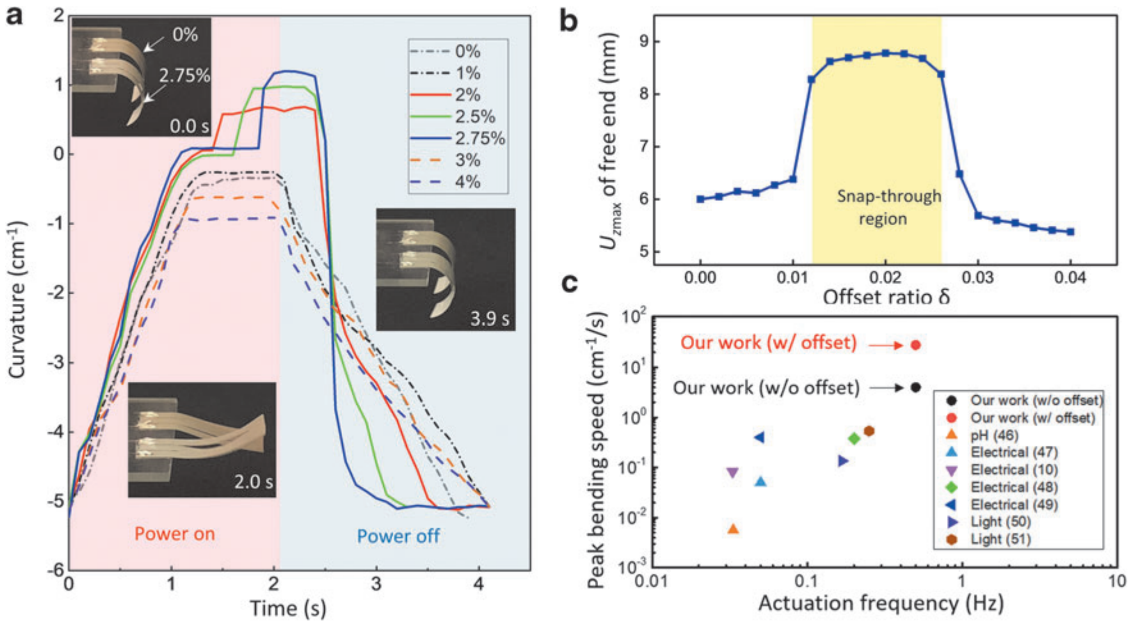

FIG. 3. Experiment and finite element analysis on the design principle of offset ratio δ. **(a)** Curvatures of the actuators with different levels of offset displacement. The *inset* photographs are snapshots of two cases ($\delta = 0\%$ and 2.75%) at different time. **(b)** FEA results of the maximum vertical displacement at the free end with different levels of offset ratio δ. **(c)** Comparison of peek bending speed between the snap-through enabled bimorph thermal actuator (our work) and other reported soft bimorph thermal actuators under different stimuli. FEA, finite element analysis. Color images are available online.

To optimize the design value of δ, we carried out a coupled thermomechanical FEA to simulate the actuation of the bimorph beams with the same initial curvature as that in experiments using ABAQUS (version 2017). A perfect bonding is assumed between the two constituent layers (AgNW/PDMS and PDMS) of the bimorph. An offset displacement is applied to the free end of the passive ribbon, while all fixed boundary conditions are assigned to the free ends of the active ribbons. A uniform body heat flux (1.38×10^9 W/m^3) is applied through the two active ribbons and the connecting part to simulate Joule heating along the conducting path.

To quantitatively evaluate the snap-through behavior, the maximum displacements of the free end of the actuator with different offset ratios are plotted (Fig. 3b). FEA results show that for successful snap through the applied offset ratio should be between 1.2% and 2.75%, which agrees well with experimental measurements.

In Figure 3c, we compare the peak bending speeds in our work and those of the reported soft bimorph thermal actuators with respect to the actuation frequency. The thermal actuators were triggered by different stimuli such as pH,[47] current (Joule heating),[10,48–50] and light.[51,52] These actuators typically showed a linear relationship of curvature and time under constant stimuli and had relatively low bending speed (0.006–0.536 cm^{-1}/s).[10,47–52] By contrast, our actuator even without introducing the snap-through mechanism (offset displacement) is already among the fastest (4.1 cm^{-1}/s). With the snap-through design, the peak bending speed is further enhanced to be over 10 times faster, that is, 28.7 cm^{-1}/s, which is over 50 times faster than the highest reported in the literature (0.536 cm^{-1}/s).[52]

The averaged bending speed within an actuation cycle is also improved (5.11 cm^{-1}/s for snap through and 4.35 cm^{-1}/s for snap back), compared with the case without snap-through mechanism. In terms of actuation frequency, our actuator yields stable performance at around 0.47 Hz, which is also higher than all the reported results. Another advantage of our soft actuator is the low operation voltage. The reported electrically powered actuator generally required input voltage ranging from 4.5 to 30 V.[10,48–50] Yet our actuator only requires 2 V to achieve the high-speed actuation.

To provide further insight into the snap-through mechanism, we conducted another FEA to examine the mechanical response of the bimorph actuator (Supplementary Fig. S5). All boundary conditions are similar to those in the previous thermomechanical FEA. Offset displacement ($\delta = 0\%$ and $\delta = 2\%$) is applied to the free end of the passive ribbon (point A in Supplementary Fig. S5). Then a displacement-controlled loading condition in z-direction is assigned to the free end of the passive ribbon (point B in Supplementary Fig. S5), and the reaction force at the same point is calculated. The force-displacement curve at point B and the corresponding snapshots capture the snap-through behavior. The force decrease during the snap through reflects release of the strain energy in the structure, which is a typical manifestation of the snap-through instability.[53]

To harness the fast response of the bistable thermal bimorph for potential applications, we first demonstrated an entirely soft crawling robot with high locomotion speed. The soft crawling robot is similar to the bimorph thermal actuator in structure but with the addition of four extended limbs on the four ends of the active ribbons. This limb design extends the front and back ends of the soft robot, which amplifies the bending amplitude in each actuation cycle and increases the crawling speed. A piece of adhesive tape was used to secure the displaced passive ribbon (with offset ratio δ) together with active ribbons. Figure 4a schematically shows the actuation procedure where a square waved voltage is supplied. The electrical power required for the crawling robot is around 0.22–0.26 W.

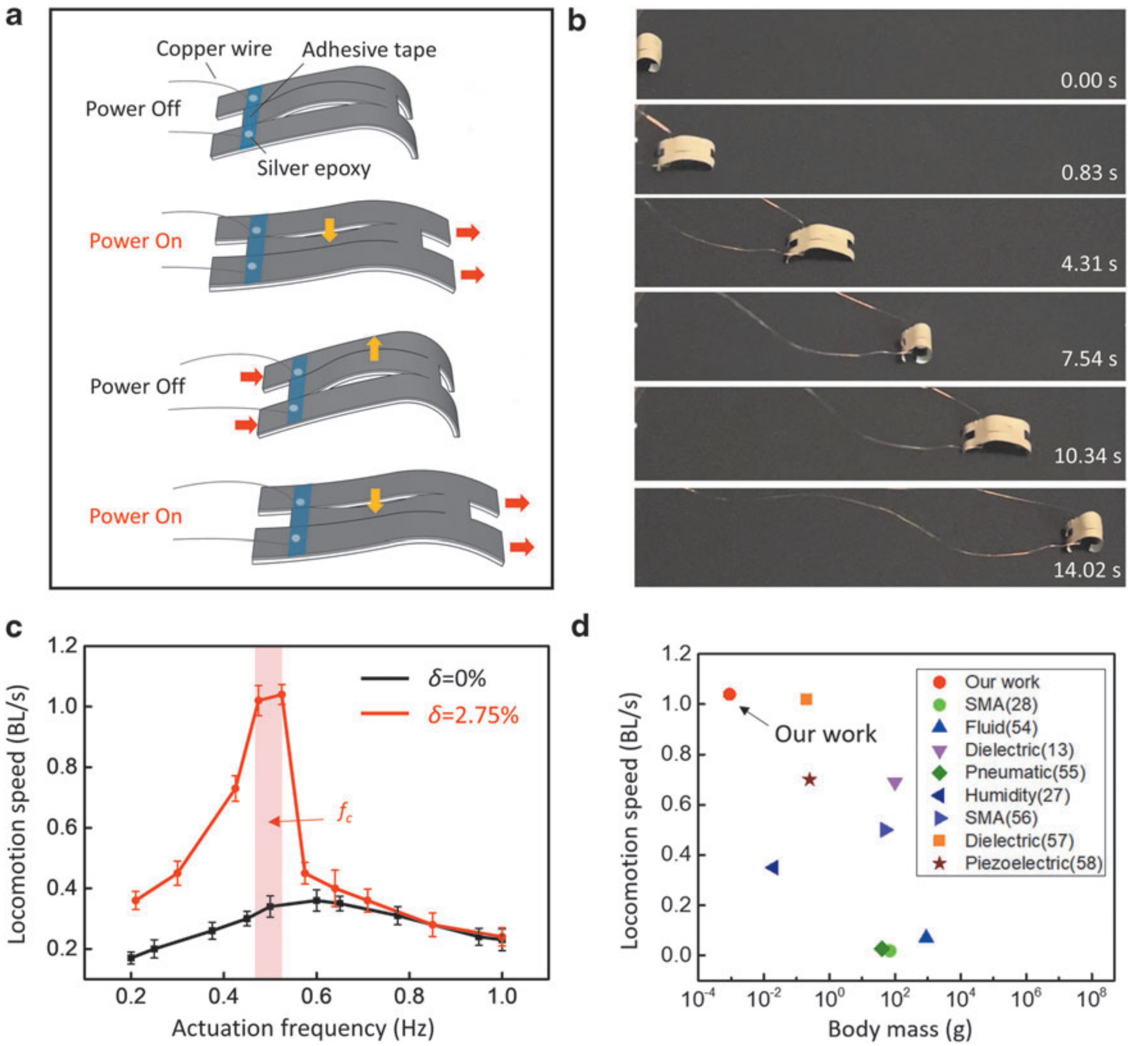

FIG. 4. Snap-through enabled high-speed crawling robot. **(a)** Schematic illustration of the locomotion. **(b)** Live snapshots showing motion of a snap-through enabled crawling robot. **(c)** Comparison between two cases on the locomotion speeds with respect to the actuation frequency. **(d)** Comparison on the locomotion speed and body mass between the high-speed crawling robots (this work) and other reported soft locomotion robots (solid symbols for on-land robots and open symbol for under-water robot). Color images are available online.

Since a constant voltage is applied, introducing the snap-through mechanism actually reduces the power consumption by reducing the time required for reaching the same degree of bending curvature. When the power is on, the middle passive ribbon goes through the bending and snap-through process as described earlier and pushes the front limbs forward. When the power is off, the passive ribbon snaps back and brings the back limbs forward.

Of note is the friction difference between the front and back limbs. Most existing crawling robots adopted special asymmetrical designs either on the crawling feet or on the ground to achieve unidirectional locomotion.[10,54] In our case, no asymmetric design on the feet is needed. The end with adhesive tape bends less than the other end because the scotch tape increases the bending stiffness (Fig. 4a). As a result, the pointing angles of the front end and the back end against the ground are different, leading to different levels of friction. Figure 4b shows a series of snapshots that captured the crawling motion within 14 s.

The actuation frequency is a key factor that determines the actuation speed. In this study, we investigated the effect of the actuation frequency on the crawling speed of the robot ($\delta = 2.75\%$) as shown in Figure 4c.

In addition, Figure 4c shows the enhancement in the locomotion speed by introducing the offset displacement, compared to the no-offset case. The maximum location speed is achieved at the frequency between 0.47 and 0.52 Hz (defined as critical frequency f_c), which agrees well with the aforementioned experimental and simulation results on the bimorph thermal actuator. When the actuation frequency is lower than f_c, the time gap between the snap-forward and snap-back instabilities is too long and hence the speed is not fully exploited; when the actuation frequency is higher than f_c, the actuation time is not sufficient for the actuator to reach the transition temperature T_H and T_L (i.e., overcome the energy barriers for the snap through). Within the critical frequency range, the locomotion speed of the soft crawling robot in this work reached 1.04 BL/s.

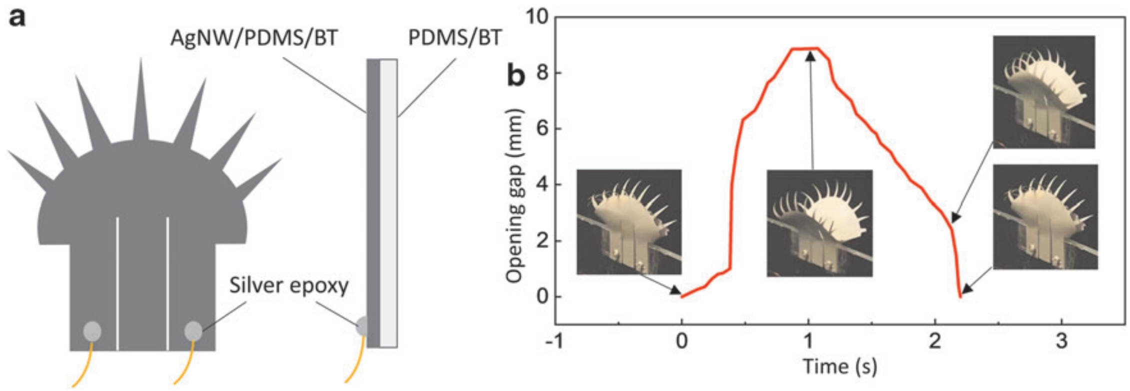

FIG. 5. Snap-through enabled biomimetic Venus flytrap. **(a)** Schematic design of the snap-through enabled biomimetic Venus flytrap. **(b)** Measured opening width of the biomimetic flytrap versus time with *inset* snapshots at different time. Color images are available online.

For comparison, the crawling robots without offset yield a locomotion speed range of 0.19–0.36 BL/s. In Figure 4d, we compare our crawling robot with entirely soft robots (solid symbols for on-land robots and open symbol for under-water robot) in the literature in terms of locomotion speed and body mass.[13,26,27,55–59] Here an entirely soft robot is defined as without rigid internal structures. It can be seen that our robot is among the fastest of the entirely soft crawling robots. Of note is that as shown in Figure 4d, the dielectric material enabled crawling robot yielded the same level of locomotion speed (1.03 BL/s) but the body mass was over 200 times that of our robot. Not to mention that it required a very high voltage (e.g., 3 kV),[58] while our crawling robot requires only 2 V.

As the second demonstration, we developed a biomimetic device that imitates a Venus flytrap. As shown in Figure 5a, a semicircle shape with multiple pointy thorns is designed imitating the lobes of a Venus flytrap. The three-ribbon structure (with $\delta = 2.75\%$) provides fast opening and closing of the lobes. Figure 5b illustrates the measured opening gap of the biomimetic flytrap as a function of time during one cycle of actuation. The opening and closing each take ~ 1 s with the tip speed up to 24 mm/s, which is close to the speed of a real Venus flytrap (0.5–1 s). Interestingly, the closing process of our biomimetic flytrap follows the same process as real Venus flytraps, that is, starting with a slow speed and then suddenly speeding up.[60] This snap-through structure may provide insights to other high-performance biomimetic designs.

Conclusions

In summary, this work reported a novel approach to increase the speed of soft thermal actuators, which has been a bottleneck limiting their application in fast soft robots. We designed and fabricated the bimorph thermal actuator with AgNW/PDMS composite film as the heating material and exploited snap-through instability to significantly increase the actuation speed.

The effect of BT doping in the AgNW/PDMS composite, offset displacement, and actuation frequency was studied to improve the actuator performance. The snap-through instability played a critical role in increasing the actuation speed. The actuator yielded a bending speed as high as 28.7 cm^{-1}/s, 10 times that without the snap-through instability and >50 times faster than the highest reported in the literature. FEA was conducted to optimize the offset ratio and provide further insight into the snap-through mechanism.

Finally, we demonstrated the usability of the bimorph thermal actuator with a fast-moving soft crawling robot (1.04 BL/s) and a biomimetic Venus flytrap. This snap-through mechanism reported in this work can be extended to increasing the speed of other types of soft actuators and robots.

Associated Content

Supporting information

Additional figures included thermal conductivity of BT/PDMS composite samples (Supplementary Fig. S1); temperature cycle of the AgNW/PDMS composite film under 0.5, 1, 1.5, 2, and 2.2 V as a result of joule heating; temperature cycle of the AgNW/PDMS composite film with and without BT (80% weight ratio) doping under 2 V joule heating (Supplementary Fig. S2); CTE of AgNW/PDMS composites with different AgNW densities (Supplementary Fig. S3); temperature and curvature of the snap-through enabled bimorph thermal actuator in six cycles (including the first) (Supplementary Fig. S4); and FEA results of the force-displacement curves at point B under a displacement-controlled loading condition in z-direction for $\delta = 0\%$ and 2%. The inset snapshots are displacement contours of the structure at different stages of the deformation for $\delta = 0\%$ and 2% (Supplementary Fig. S5).

Additional movies included comparison of the bending motion between the bimorph thermal actuators with no-offset and 2.75% offset (Supplementary Movie S1); top view of the snap-through enabled high-speed crawling robot (Supplementary Movie S2); tilted view of the snap-through enabled high-speed crawling robot (Supplementary Movie S3); comparison of the snap-through enabled crawling robots with no-offset and 2.75% offset (Supplementary Movie S4); and demonstration of the snap-through enabled biomimetic Venus flytrap (Supplementary Movie S5). (MP4).

Authors' Contributions

S.W. and Y.Z. designed the research. S.W. and G.L.B. performed the research. S.W., G.L.B., J.Y., and Y.Z. analyzed the data. S.W. and Y.Z. wrote the article.

Author Disclosure Statement

No competing financial interests exist.

Funding Information

The work was supported, in part, by the National Science Foundation through Award No. IIS-1637892.

Supplementary Material

Supplementary Figure S1
Supplementary Figure S2
Supplementary Figure S3
Supplementary Figure S4
Supplementary Figure S5
Supplementary Movie S1
Supplementary Movie S2
Supplementary Movie S3
Supplementary Movie S4
Supplementary Movie S5

References

1. Rus D, Tolley MT. Design, fabrication and control of soft robots. Nature 2015;521:467–475.
2. Rich SI, Wood RJ, Majidi C. Untethered soft robotics. Nat Electron 2018;1:102–112.
3. Morin SA, Shepherd RF, Kwok SW, *et al.* Camouflage and display for soft machines. Science 2012;337:828–832.
4. Mutlu R, Alici G, in het Panhuis M, *et al.* 3D printed flexure hinges for soft monolithic prosthetic fingers. Soft Robot 2016;3:120–133.
5. Gorissen B, Reynaerts D, Konishi S, *et al.* Elastic inflatable actuators for soft robotic applications. Adv Mater 2017;29:1604977.
6. Cianchetti M, Laschi C, Menciassi A, *et al.* Biomedical applications of soft robotics. Nat Rev Mater 2018;3:143–153.
7. Thuruthel TG, Shih B, Laschi C, *et al.* Soft robot perception using embedded soft sensors and recurrent neural networks. Sci Robot 2019;4:eaav1488.
8. Tolley MT, Shepherd RF, Mosadegh B, *et al.* A resilient, untethered soft robot. Soft Robot 2014;1:213–223.
9. Shepherd RF, Ilievski F, Choi W, *et al.* Multigait soft robot. PNAS 2011;108:20400–20403.
10. Yao S, Cui J, Cui Z, *et al.* Soft electrothermal actuators using silver nanowire heaters. Nanoscale 2017;9:3797–3805.
11. He Q, Wang Z, Wang Y, *et al.* Electrically controlled liquid crystal elastomer-based soft tubular actuator with multimodal actuation. Sci Adv 2019;5:eaax5746.
12. Acome E, Mitchell S, Morrissey T, *et al.* Hydraulically amplified self-healing electrostatic actuators with muscle-like performance. Science 2018;359:61–65.
13. Li T, Li G, Liang Y, *et al.* Fast-moving soft electronic fish. Sci Adv 2017;3:e1602045.
14. Shintake J, Cacucciolo V, Floreano D, *et al.* Soft robotic grippers. Adv Mater 2018;30:1707035.
15. Hu W, Lum GZ, Mastrangeli M, *et al.* Small-scale soft-bodied robot with multimodal locomotion. Nature 2018;554:81–85.
16. Mao G, Drack M, Karami-Mosammam M, *et al.* Soft electromagnetic actuators. Sci Adv 2020;6:eabc0251.
17. Kim Y, Yuk H, Zhao R, *et al.* Printing ferromagnetic domains for untethered fast-transforming soft materials. Nature 2018;558:274–279.
18. Nawroth JC, Lee H, Feinberg AW, *et al.* A tissue-engineered jellyfish with biomimetic propulsion. Nat Biotechnol 2012;30:792–797.
19. Must I, Sinibaldi E, Mazzolai B. A variable-stiffness tendril-like soft robot based on reversible osmotic actuation. Nat Commun 2019;10:1–8.
20. Bar-Cohen Y, Zhang Q. Electroactive polymer actuators and sensors. MRS Bull 2008;33:173–181.
21. Chen L, Liu C, Liu K, *et al.* High-performance, low-voltage, and easy-operable bending actuator based on aligned carbon nanotube/polymer composites. ACS Nano 2011;5:1588–1593.
22. Kim H, Lee H, Ha I, *et al.* Biomimetic color changing anisotropic soft actuators with integrated metal nanowire percolation network transparent heaters for soft robotics. Adv Funct Mater 2018;28:1801847.
23. Hawkes E, An B, Benbernou NM, *et al.* Programmable matter by folding. PNAS 2010;107:12441–12445.
24. Yao S, Yang J, Poblete FR, *et al.* Multifunctional electronic textiles using silver nanowire composites. ACS Appl Mater Interfaces 2019;11:31028–31037.
25. Lee JW, Xu R, Lee S, *et al.* Soft, thin skin-mounted power management systems and their use in wireless thermography. PNAS 2016;113:6131–6136.
26. Shin B, Ha J, Lee M, *et al.* Hygrobot: a self-locomotive ratcheted actuator powered by environmental humidity. Sci Robot 2018;3:eaar2629.
27. Wang W, Lee J-Y, Rodrigue H, *et al.* Locomotion of inchworm-inspired robot made of smart soft composite (SSC). Bioinspir Biomim 2014;9:046006.
28. Singh V, Bougher TL, Weathers A, *et al.* High thermal conductivity of chain-oriented amorphous polythiophene. Nat Nanotechnol 2014;9:384–390.
29. Park HS, Wang Q, Zhao X, *et al.* Electromechanical instability on dielectric polymer surface: modeling and experiment. Comput Methods Appl Mech Eng 2013;260:40–49.
30. Han M, Wang H, Yang Y, *et al.* Three-dimensional piezoelectric polymer microsystems for vibrational energy harvesting, robotic interfaces and biomedical implants. Nat Electron 2019;2:26–35.
31. Chen T, Bilal OR, Shea K, *et al.* Harnessing bistability for directional propulsion of soft, untethered robots. PNAS 2018;115:5698–5702.
32. Overvelde JT, Kloek T, D'haen JJ, *et al.* Amplifying the response of soft actuators by harnessing snap-through instabilities. PNAS 2015;112:10863–10868.
33. Tang Y, Chi Y, Sun J, *et al.* Leveraging elastic instabilities for amplified performance: spine-inspired high-speed and high-force soft robots. Sci Adv 2020;6:eaaz6912.
34. Keplinger C, Li T, Baumgartner R, *et al.* Harnessing snap-through instability in soft dielectrics to achieve giant voltage-triggered deformation. Soft Matter 2012;8:285–288.
35. Chen D, Yoon J, Chandra D, *et al.* Stimuli-responsive buckling mechanics of polymer films. J Polym Sci Part B: Polym Phys 2014;52:1441–1461.
36. Rothemund P, Ainla A, Belding L, *et al.* A soft, bistable valve for autonomous control of soft actuators. Sci Robot 2018;3:eaar7986.

37. Yao S, Zhu Y. Nanomaterial-enabled stretchable conductors: strategies, materials and devices. Adv Mater 2015;27: 1480–1511.
38. Hong S, Lee H, Lee J, *et al.* Highly stretchable and transparent metal nanowire heater for wearable electronics applications. Adv Mater 2015;27:4744–4751.
39. Choi S, Park J, Hyun W, *et al.* Stretchable heater using ligand-exchanged silver nanowire nanocomposite for wearable articular thermotherapy. ACS Nano 2015;9:6626–6633.
40. Li J, Liang J, Jian X, *et al.* A flexible and transparent thin film heater based on a silver nanowire/heat-resistant polymer composite. Macromol Mater Eng 2014;299:1403–1409.
41. Ge J, Yao H, Wang X, *et al.* Stretchable conductors based on silver nanowires: improved performance through a binary network design. Angew Chem Int Ed 2013;52:1654–1659.
42. Xu F, Zhu Y. Highly conductive and stretchable silver nanowire conductors. Adv Mater 2012;24:5117–5122.
43. Song L, Myers AC, Adams JJ, *et al.* Stretchable and reversibly deformable radio frequency antennas based on silver nanowires. ACS Appl Mater Interfaces 2014;6:4248–4253.
44. Yao S, Zhu Y. Wearable multifunctional sensors using printed stretchable conductors made of silver nanowires. Nanoscale 2014;6:2345–2352.
45. Cui Z, Han Y, Huang Q, *et al.* Electrohydrodynamic printing of silver nanowires for flexible and stretchable electronics. Nanoscale 2018;10:6806–6811.
46. Huang Q, Zhu Y. Gravure printing of water-based silver nanowire ink on plastic substrate for flexible electronics. Sci Rep 2018;8:1–10.
47. Yuan P, McCracken J, Gross D, *et al.* A programmable soft chemo-mechanical actuator exploiting a catalyzed photochemical water-oxidation reaction. Soft Matter 2017;13: 7312–7317.
48. Zhao H, Hu R, Li P, *et al.* Soft bimorph actuator with real-time multiplex motion perception. Nano Energy 2020; 104926.
49. Li W, Li F, Li H, *et al.* Flexible circuits and soft actuators by printing assembly of graphene. ACS Appl Mater Interfaces 2016;8:12369–12376.
50. Taccola S, Greco F, Sinibaldi E, *et al.* Toward a new generation of electrically controllable hygromorphic soft actuators. Adv Mater 2015;27:1668–1675.
51. Chang L, Huang M, Qi K, *et al.* Graphene-based bimorph actuators with dual-response and large-deformation by a simple method. Macromol Mater Eng 2019;304:1800688.
52. Deng H, Zhang C, Su J-W, *et al.* Bioinspired multi-responsive soft actuators controlled by laser tailored graphene structures. J Mater Chem B 2018;6:5415–5423.
53. Abdullah AM, Braun PV, Hsia KJ. Programmable shape transformation of elastic spherical domes. Soft Matter 2016;12:6184–6195.
54. Wu Y, Yim JK, Liang J, *et al.* Insect-scale fast moving and ultrarobust soft robot. Sci Robot 2019;4:eaax1594.
55. Onal CD, Rus D. Autonomous undulatory serpentine locomotion utilizing body dynamics of a fluidic soft robot. Bioinspir Biomim 2013;8:026003.
56. Tang Y, Zhang Q, Lin G, *et al.* Switchable adhesion actuator for amphibious climbing soft robot. Soft Robot 2018; 5:592–600.
57. Umedachi T, Vikas V, Trimmer BA. Softworms: the design and control of non-pneumatic, 3D-printed, deformable robots. Bioinspir Biomim 2016;11:025001.
58. Duduta M, Clarke DR, Wood RJ. A high speed soft robot based on dielectric elastomer actuators. In: 2017 IEEE International Conference on Robotics and Automation (ICRA). Manhattan, NY: IEEE, 2017, pp. 4346–4351.
59. Park T, Cha Y. Soft mobile robot inspired by animal-like running motion. Sci Rep 2019;9:1–9.
60. Stuhlman O. A physical analysis of the opening and closing movements of the lobes of Venus' fly-trap. Bull Torrey Bot 1948;75:22–44.

Address correspondence to:
Yong Zhu
Department of Mechanical and Aerospace Engineering
North Carolina State University
Raleigh, NC 27695-7910
USA

E-mail: yong_zhu@ncsu.edu